Scattering of High-Energy Electrons by Nitrogen-14 and -15*

E. B. Dally†
High Energy Physics Laboratory, Stanford University, Stanford, California 94305

and

M. G. Croissiaux
High Energy Physics Laboratory, Stanford University, Stanford, California 94305 and Institut de Recherches Nucléaires, Strasbourg, France

and

B. Schweitz
Institut de Recherches Nucléaires, Strasbourg, France

(Received 22 May 1970)

Cross sections of elastic and inelastic electron scattering at incident electron energies of 250 and 400 MeV are presented. Data are given for elastic and inelastic scattering from N^{15} and elastic scattering from N^{14}. The data are analyzed with the use of the shell model, in Born approximation. The rms radius of N^{14} is found to be 2.64 F at 400 MeV. The rms radius of N^{15} at 250 and 400 MeV is 2.65 and 2.63 F, respectively. Excited levels in N^{15} at 5.3, 6.3, and 7.3 MeV are studied. Values of the nuclear transition probabilities are presented for these levels. The spin and parity assignments made are $J^\pi = \frac{5}{2}^+$ and $J^\pi = \frac{1}{2}^+$ for the doublet at 5.3 MeV. The 6.3-MeV level is assigned $J^\pi = \frac{3}{2}^-$. Of the triplet of levels at 7.3 MeV, only the 7.3- and 7.5-MeV levels are strongly excited. These agree with $J^\pi = \frac{3}{2}^+$ and $J^\pi = \frac{7}{2}^+$, respectively.

INTRODUCTION

Recently we have presented results concerning measurements of the elastic electron scattering by the N^{15} isotope.[1] The data were analyzed by a phase-shift calculation using two phenomenological models. We used the Fermi model (with two and three parameters) and a simplified version of the shell model (with two parameters a and α). It was found that a good fit could be made on both sides of the diffraction minimum but not at the diffraction dip. We present another analysis, here, which uses a complete version of the shell model in the Born approximation. We also present results on the electron scattering from N^{14} obtained during the same data runs. We have analyzed the data by the same method and compare the radii of N^{14} and N^{15}.

When we measured the elastic scattering cross sections for N^{15}, we accumulated data on the inelastic scattering to the low-lying excited levels to an excitation up to 8 or 9 MeV. We give the cross sections and angular distributions corresponding (1) to the doublet at 5.28 and 5.30 MeV, (2) to the level at 6.3 MeV, and (3) to the second two of the three unresolved levels at 7.16, 7.31, and 7.56 MeV.

In Sec. I, some experimental details and the extraction of cross sections for the levels are given. In Sec. II, the formalism used to analyze the data is developed, and the expressions for a comparison with the experiment are given. Section III describes the analysis of the data and the results are discussed.

The experimental setup was explained in the previous article[1] for the elastic e-N^{15} scattering. The same method was used for the elastic e-N^{14} and the inelastic e-N^{15} measurements.

I. DATA REDUCTION

The data for inelastic N^{15} scattering were treated by the same method used in Ref. 1. The detection apparatus has an energy resolution of about 0.08%, but this is not sufficient to resolve all the levels. A typical spectrum of the N^{15} electron scattering spectrum is displayed in Fig. 1. The inelastic spectrum shows three peaks. The peak labeled a refers to the doublet at 5.276 and 5.304 MeV. The peak b corresponds to the level at 6.328 MeV. The third peak has the contribution of the three levels located at 7.16 MeV (c), at 7.31 MeV (d), and at 7.57 MeV (e). The position of this third peak corresponds mainly to the level e, indicating that the cross sections for the levels c and d are less important.

We have assumed that the spectra are the sum of Gaussian curves and have calculated the contribution of each peak with a least-squares-fit program. A typical example is shown in Fig. 2. This

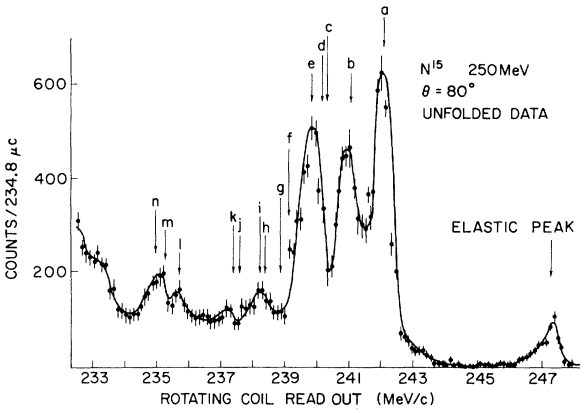

FIG. 1. An elastic and inelastic electron scattering spectrum of N^{15} taken at 250 MeV using the 100-channel ladder apparatus. The positions of the inelastic levels are indicated by the letters. Those that are analyzed and described in the text are a, b, d, and e.

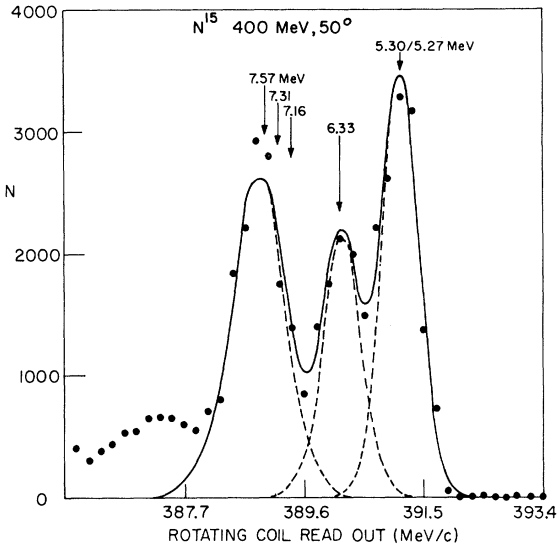

FIG. 2. The position of the inelastic N^{15} spectrum containing the inelastic levels that are analyzed. The dashed curves are the unfolded Gaussian curves of the three groups of levels analyzed. N is the counting rate in arbitrary units. The procedure is described in the text.

method is an approximation because the third peak is actually the sum of unequal contributions from three levels. But, in most cases, the sum of the three calculated Gaussian curves reproduced the experimental spectrum very well, and each of the Gaussian curves had the right position and about the same spectral width. In some cases, that method gave a bad fit. This happened when the statistical accuracy was poor and/or the middle peak (b) was small in comparison with the other ones. In these instances some contribution from the 7.16-MeV level (small compared with the 7.57 level) was counted with the 6.31-MeV-level contribution and not with the 7.57 level. In those cases, a manual fit was done and the errors have been increased.

When the number of counts in each peak had been determined, the cross sections were calculated relative to the elastic cross sections.

The statistical errors for these excited-level cross sections have been calculated by taking into account the error of the elastic cross sections and the error on the statistics of the inelastic peak. The last error is already a combination of the statistical error of the peak and the uncertainty in the separation of each peak in the experimental curves.

The results are given in Tables I, II, and III, which contain form factors and cross sections for

TABLE I. Elastic electron scattering cross sections and form factors for N^{14} at 250- and 400-MeV incident electron energy.

250				400			
θ (deg)	q (F^{-1})	$10^{33}\times\frac{d\sigma}{d\Omega}$ (cm^2/sr)	$10^4\times F^2(q^2)$	θ (deg)	q (F^{-1})	$10^{33}\times\frac{d\sigma}{d\Omega}$ (cm^2/sr)	$10^4\times F^2(q^2)$
40	0.86	42 706 ± 1640	1643 ± 63	32	1.12	12 665 ± 380	500 ± 15
45	0.97			35	1.22	4600 ± 120	261 ± 7
50	1.07	6627 ± 165	637 ± 16	38	1.32	1511 ± 51	120 ± 4
55	1.17			40	1.38	747 ± 24	73.2 ± 2.3
60	1.26	943.7 ± 29	195 ± 6				
65	1.35			43	1.48	218 ± 7	28.8 ± 0.9
70	1.45	105.2 ± 3	42.3 ± 1.2	45	1.55	93.4 ± 3	14.7 ± 0.5
75	1.53			48	1.64	29.6 ± 0.9	6.18 ± 0.19
80	1.62	10.8 ± 8	7.25 ± 0.54	50	1.70	14.4 ± 0.4	3.56 ± 0.10
82	1.65			53	1.80	9.60 ± 0.4	3.03 ± 0.13
84	1.62			55	1.86	9.00 ± 0.3	3.32 ± 0.11
90	1.78	2.8 ± 0.2	3.50 ± 0.31	65	2.16	4.56 ± 0.2	3.43 ± 0.15
100	1.92			75	2.44	1.22 ± 0.08	1.72 ± 0.11
105	1.99			80	2.58	0.425 ± 0.041	0.799 ± 0.076
110	2.05			85	2.70	0.125 ± 0.02	0.310 ± 0.060

TABLE II. Elastic electron scattering cross sections and form factors for N^{15} at 250- and 400-MeV incident electron energy.

250				400			
θ (deg)	q (F^{-1})	$10^{33}\times\frac{d\sigma}{d\Omega}$ (cm^2/sr)	$10^4\times F^2(q^2)$	θ (deg)	q (F^{-1})	$10^{33}\times\frac{d\sigma}{d\Omega}$ (cm^2/sr)	$10^4\times F^2(q^2)$
40	0.26	37 700 ± 2400	1443 ± 90	32	1.15	11 260 ± 510	445 ± 21
45	0.97	13 600 ± 800	845 ± 50	35	1.22	3540 ± 150	202 ± 9
50	1.07	4650 ± 300	448 ± 29	38	1.32	1127 ± 45	89.8 ± 3.6
55	1.17	1960 ± 118	281 ± 17	40	1.38	536 ± 21	52.7 ± 2.1
60	1.26	691 ± 44	143 ± 9	42	1.45	189 ± 87	22.7 ± 1.0
65	1.35	210 ± 13	61 ± 3.7	43	1.48		
70	1.45	47.7 ± 2.9	19.1 ± 1.1	45	1.55	41.8 ± 1.5	6.74 ± 0.25
75	1.53	14.2 ± 0.85	7.72 ± 0.46	48	1.64	6.88 ± 0.40	1.44 ± 0.09
80	1.62	3.10 ± 0.19	2.25 ± 0.14	50	1.70	4.87 ± 0.20	1.20 ± 0.06
82	1.65	2.12 ± 0.13	1.72 ± 0.11	53	1.80	6.51 ± 0.38	2.05 ± 0.13
84	1.67	2.07 ± 0.15	1.88 ± 0.14	55	1.86	8.19 ± 0.27	3.02 ± 0.10
85	1.70			58	1.95	8.12 ± 0.29	3.74 ± 0.15
86	1.71	2.06 ± 0.13	2.08 ± 0.14	60	2.01	7.70 ± 0.22	4.10 ± 0.14
90	1.78	2.15 ± 0.17	2.69 ± 0.21	65	2.16	4.91 ± 0.14	3.68 ± 0.13
95	1.85	2.57 ± 0.15	4.17 ± 0.25	70	2.30	2.05 ± 0.082	2.12 ± 0.09
100	1.92	2.40 ± 0.14	5.02 ± 0.29	75	2.44	0.890 ± 0.046	1.20 ± 0.07
105	1.99	2.08 ± 0.12	5.59 ± 0.34	80	2.58	0.340 ± 0.015	0.64 ± 0.03
110	2.05	1.37 ± 0.10	4.72 ± 0.32	85	2.70		

N^{14} elastic scattering, N^{15} elastic scattering, and N^{15} inelastic scattering, respectively. Figure 3 shows a typical N^{14} spectrum. The lowest excited level of N^{14} is well resolved from the elastic peak. The form factors [defined as shown in Eq. (1) below] are plotted in Figs. 4–8. The form factors for the inelastic levels are given in Table IV.

II. THEORETICAL ANALYSIS

Evaluation of the theoretical cross section for electron-nucleus scattering has been extensively studied by the first Born approximation.[2-4] The approximation is expected to be good when $Z\alpha \ll 1$, where α is the fine-structure constant. In the case of nitrogen, $Z\alpha \simeq 0.05$, so that the approximation should be valid. One should point out another restriction. To evaluate the nuclear matrix elements, it is assumed that the nucleus can be treat-

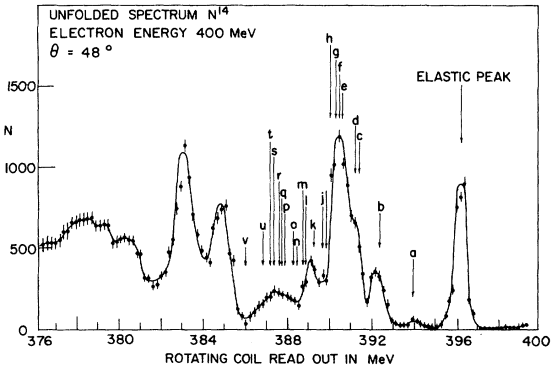

FIG. 3. The same as Fig. 1 for N^{14}.

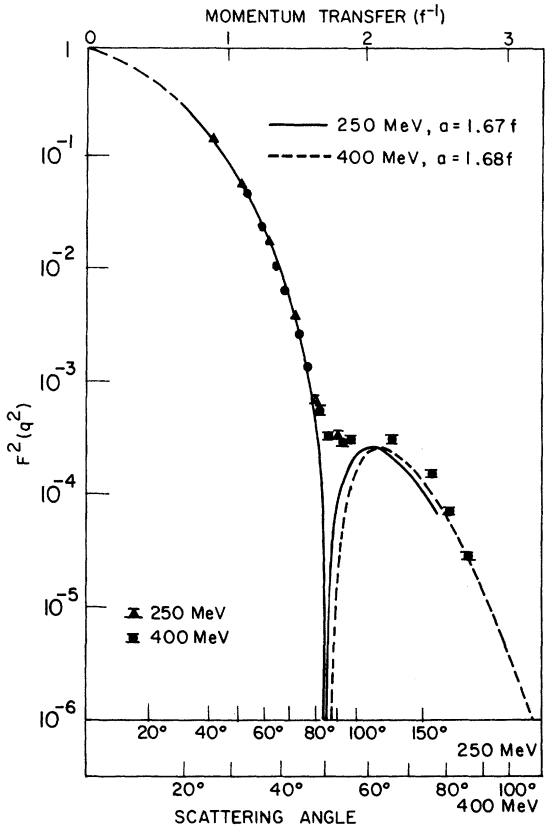

FIG. 4. The form factor versus momentum transfer from the elastic scattering of electrons from N^{14} at 250 and 400 MeV. The curves are the results of a monopole fit to the data. See text for description.

TABLE III. Inelastic electron scattering cross sections from N^{15} at 250 and 400 MeV for the doublet level at 5.3 MeV, the 6.3-MeV level, and the triplet level at 7.3 MeV.

E_0 (MeV)	θ (deg)	$10^{33}\times d\sigma/d\Omega$ 5.3-MeV levels	6.3-MeV levels	7.3-MeV levels
250	45	311±31	451±39	296±38
	50	221±32	271±43	200±44
	55	149±24	160±17	140±24
	60	76±11	98±13	83±12
	65	57±9	65±9	48±6.7
	70	39±6	35.4±5	37.4±5
	75	28.5±4	26.6±4	31.7±5
	80	19.8±3	15.4±2	21.6±3
	82	16.6±2	10.5±1.5	19.1±2
	84	13.2±2	7.5±1.3	18.7±3
	85	12.7±2.4	6.5±2.0	16.0±3
	86	9.95±1.4	8.7±1.3	13.9±2
	90	8.28±1.3	4.8±0.7	10.4±1.5
	95	4.80±0.7	4.01±0.6	5.3±0.8
	100	3.19±0.54	2.16±0.3	3.9±0.6
	105	2.20±0.35	0.99±0.2	2.78±0.5
	110	1.78±0.4	0.41±0.13	1.64±0.4
400	32	613±95	475±11	458±103
	35	262±34	385±52	291±41
	38	220±20	266±30	247±27
	40	173±22	189±22	231±25
	42	140±10	122±15	154±21
	45	88.4±9	76±6	103±9
	48	56.8±4	41±4	67±7
	50	43.3±5	26±3	49±6
	53	25.8±3	15.0±2	33±4
	55	18.3±3	12.6±2	21±2.5
	58	10.5±1	5.19±0.9	13.3±2
	60	6.30±1	3.33±0.8	9.04±1.3
	65	3.04±0.7	1.36±0.4	3.76±0.5
	70	0.85±0.2	0.30±0.08	1.38±0.2
	75	0.33±0.08	0.14±0.04	0.36±0.09
	80	0.19±0.05	0.04±0.01	0.18±0.05

ed nonrelativistically.[3] This assumption limits the range of momentum transfers which can be used within the framework of the present analysis. For independent-particle excitations this limit is given by $(q/M)^3 \ll 1$ (M is the nucleon mass and q is the momentum transfer). For this experiment $(q/M)^3 = 0.15$ for the highest q. Some relativistic effects might appear at the higher q's for independent-particle excitation. Using these assumptions, the differential cross section can be written as

$$\frac{d\sigma}{d\Omega} = \left(\frac{d\sigma}{d\Omega}\right)_0 F^2(q^2, \theta), \tag{1}$$

with

$$\left(\frac{d\sigma}{d\Omega}\right)_0 = \left(\frac{d\sigma}{d\Omega}\right)_{\text{Mott}} \left[1 + \frac{E_0}{Mc^2}(1-\cos\theta)\right]^{-1}. \tag{2}$$

The second factor in Eq. (2) arises from the recoil of the nucleus. The form factor F can be developed as

$$F^2(q^2, \theta) = F_L{}^2(q^2) + (\tfrac{1}{2} + \tan^2\tfrac{1}{2}\theta) F_T{}^2(q^2), \tag{3}$$

where the form factors $F_L{}^2(q^2)$ (longitudinal or Coulomb term) and $F_T{}^2(q^2)$ (transverse term) are functions of q^2 only and can be decomposed into several multipole contributions according to the selection rules and the transitions. The usual expansions are

$$F_L{}^2(q^2) = \sum_{\lambda=0}^{\infty} F_{C\lambda}{}^2(q^2) \tag{4}$$

and

$$F_T{}^2(q^2) = \sum_{\lambda=1}^{\infty} [F_{E\lambda}{}^2(q^2) + F_{M\lambda}{}^2(q^2)]. \tag{5}$$

We have chosen to compare the experimental results by using the shell model, which usually gives

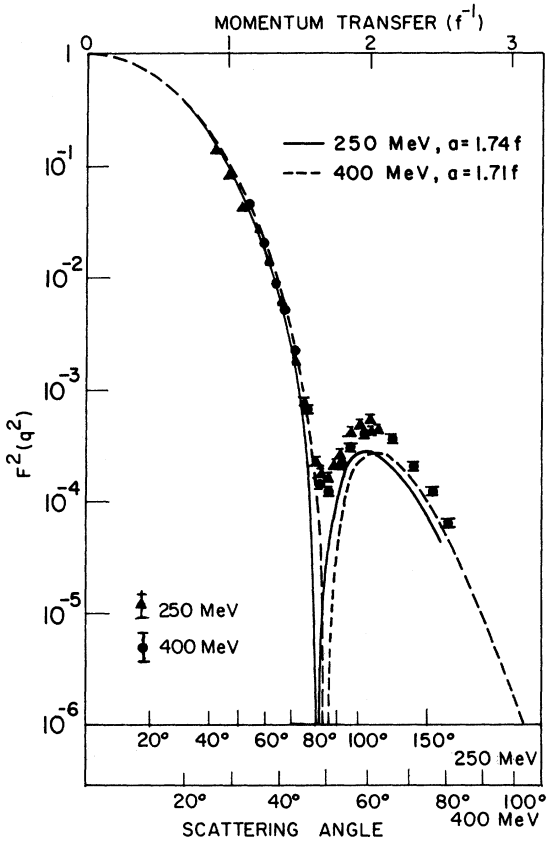

FIG. 5. The same as Fig. 4, for the elastic scattering from N^{15}.

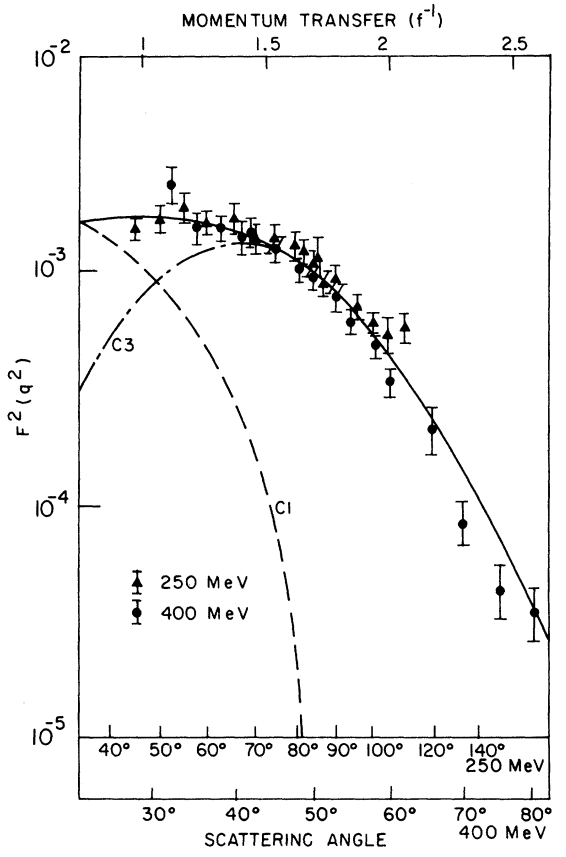

FIG. 6. The form factor versus momentum transfer for the inelastic electron scattering to the 5.3-MeV doulet in N^{15}. The curves labeled $C1$ and $C3$ are the separate contributions to the form factor of these transitions. The magnitude of each is found from a fit to the data as described in the text. The solid curve is the sum of the two transitions.

good predictions for nuclei of the p shell. The elastic scattering gives the charge distribution and some other static properties such as the magnetic moment and electric quadrupole moment.

For the inelastic scattering, the fits lead to curves giving the values of the transition probabilities for the range of q studied. The nuclear transition probabilities that are measured with real photons or by Coulomb excitation with heavy particles are given by the extrapolation of the curves to a momentum transfer of zero. The multipole terms have been explicitly calculated by Willey[3] for the shell model and developed for several nuclei.[5] With the following notation, the terms used for the present analysis are indicated below:

$$|F_{C0}(q^2)|^2 = \left|\left(1 - \frac{2}{3}\frac{Z-2}{Z}x\right)e^{-(x+d)}\right|^2, \tag{6}$$

$$|F_{C1}(q^2)|^2 = \alpha|\langle 1p|j_1|1d\rangle e^{-d}|^2,$$

$$= \alpha\left|\frac{\sqrt{10x}}{3}(1 - \tfrac{2}{5}x)e^{-(x+d)}\right|^2, \tag{7}$$

$$|F_{C2}(q^2)|^2 = \alpha|\langle 1p|j_2|1p\rangle e^{-d}|^2,$$

$$= \alpha|\tfrac{2}{3}x\, e^{-(x+d)}|^2, \tag{8}$$

$$|F_{C3}(q^2)|^2 = \beta|\langle 1p|j_3|1d\rangle e^{-d}|^2,$$

$$= \beta|x^{3/2}e^{-(x+d)}|^2, \tag{9}$$

and

$$|F_{M1}(q^2)|^2 = |\beta\langle 1p|j_0|1p\rangle\sqrt{x}\,e^{-d} + \gamma\sqrt{x}\,e^{-d}\langle 1p|j_2|1p\rangle|^2,$$

$$= x|\beta(1 - \tfrac{2}{3}x)e^{-(x+d)} + \tfrac{2}{3}\gamma x\, e^{-(x+d)}|^2 \tag{10}$$

with

$$x = \tfrac{1}{4}q^2a^2,$$

and

$$d = \tfrac{1}{4}q^2(a_p^2 - a^2/A).$$

a is the parameter of the harmonic oscillator, a_p is related to the mean radius of the proton $a_p = \frac{2}{3}(\langle r_p^2\rangle)^{1/2} = 0.63$ F, A is the atomic number, and d takes into account a correction for the finite size of the proton and recoil corrections evaluated by

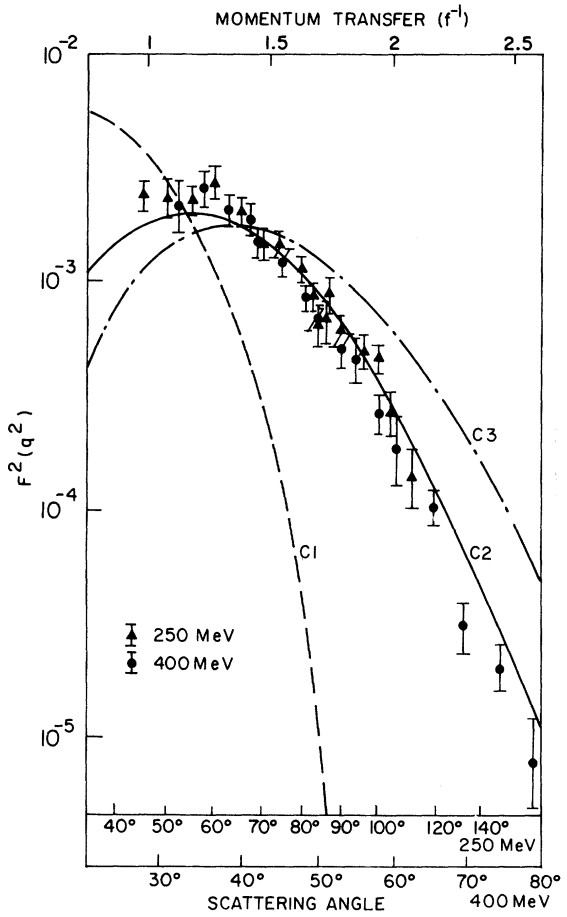

FIG. 7. The same as Fig. 5, for the excitation to the 6.3-MeV level in N^{15}. The curves $C1$, $C2$, and $C3$ are fitted to the data to find which multipole transition is involved in the excitation.

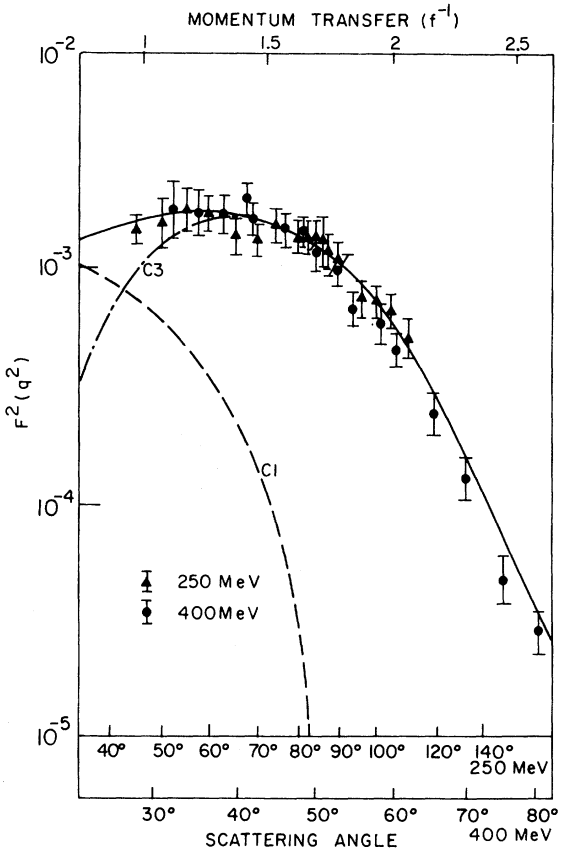

FIG. 8. The same as Fig. 5 for the excitation to the triplet of levels at 7.3 MeV in N^{15}. The curves have the same significance as in Fig. 5. Only two levels are excited strongly.

Tassie and Barker.[6] α, β, and γ are coefficients depending upon the characteristics of the nuclear transition, and are determined by a fit to the data.

A. Elastic Scattering

For the elastic scattering, the number of the multipoles that we have to deal with is restricted by the selection rules. The initial and final states are identical. Only the terms $C0$, $M1$, and $C2$ are possible. Furthermore, it is convenient to express explicitly static characteristics of the nuclei such as the magnetic dipole moment μ and the electric quadrupole moment Q. In this case, the terms that are fitted are

$$F_{C0}^2(q^2) \quad \text{[identical to Eq. (6)]},$$

$$F_{C2}^2(q^2)=\frac{q^4}{180}\frac{(J+1)(2J+3)}{J(2J-1)}\left(\frac{Q}{Z}\right)^2 e^{-2(x+d)}, \tag{11}$$

and

$$F_{M1}^2(q^2)=\frac{2}{3}\frac{J+1}{J}\frac{x}{a^2m_p^2}\left(\frac{\mu}{Z}\right)^2\left[1-\tfrac{2}{3}x+\alpha\tfrac{2}{3}x\right]^2 e^{-2(x+d)}, \tag{12}$$

where J is the angular momentum of the ground state of the nucleus, and m_p is the nucleon mass. Normally, at low momentum transfers, the first term F_{C0} (monopole term) is predominant. When only that term is present, the corresponding rms radius is

$$\langle r^2\rangle = a^2\left(\frac{5Z-4}{2Z}\right)+\frac{3}{2}\left(a_p^2-\frac{a^2}{A}\right). \tag{13}$$

In the fit by the shell model in the previous article,[1] only the first term F_{C0} was used, and a parameter α replaced the quantity $\frac{1}{3}(Z-2)$.

B. Inelastic Scattering

The general formalism indicated above is applicable to the study of the inelastic levels. Because

TABLE IV. Form factors for inelastic electron scattering at 250 and 400 MeV from excited levels at 5.3, 6.3, and 7.3 MeV.

E_0 (MeV)	θ (deg)	$10^4 \times F^2(q^2)$ 5.3-MeV levels	6.3-MeV levels	7.3-MeV levels
250	45	17.1±2	24.8±2	16.2±2
	50	19.1±3	23.5±4	17.4±4
	55	21.3±3.4	23.0±3	20.0±3
	60	18.1±3	26.6±4	19.8±3
	65	19.0±3	20.6±3	15.4±2
	70	15.9±2.5	14.3±2	15.1±2
	75	15.6±2.3	14.6±2	17.3±2.6
	80	14.5±1.9	11.3±1.5	15.9±2
	82	13.7±1.7	8.64±1.3	15.8±1.7
	84	12.0±1.7	6.81±1.2	15.9±2.4
	85	12.4±2.4	6.34±1.9	15.5±2.5
	86	9.95±1.4	8.74±1.3	13.9±2
	90	10.4±1.6	6.00±0.9	12.9±2
	95	7.76±1.2	4.96±0.7	8.56±1.3
	100	6.68±1.1	4.52±0.7	8.24±1.3
	105	5.91±1	2.66±0.6	7.49±1.2
	110	6.17±1.3	1.43±0.5	5.70±1.3
400	32	27.2±4	21.1±5	20.4±4.6
	35	17.3±2	25.3±3	19.1±2.7
	38	17.2±2	20.8±2	19.3±2
	40	16.1±2	18.7±2	22.9±2.5
	42	16.4±1.2	14.4±2	18.1±2.5
	45	14.1±1.4	12.1±0.9	16.5±1.5
	48	11.6±0.9	8.4±0.8	13.6±1.4
	50	10.7±1.2	6.5±0.7	12.2±1.5
	53	8.54±1.1	5.0±0.7	11.1±1.3
	55	6.73±1.1	4.6±1	7.70±0.9
	58	5.25±0.6	2.6±0.4	6.66±1
	60	3.50±0.6	1.9±0.4	5.02±0.7
	65	2.29±0.6	1.02±0.3	2.82±0.4
	70	0.87±0.2	0.31±0.08	1.43±0.2
	75	0.46±0.1	0.20±0.06	0.51±0.1
	80	0.36±0.09	0.076±0.02	0.34±0.1

of the fact that the initial and final states are different and can have different angular momenta, the selection rules give terms not present for elastic scattering. In addition we make the following remarks:

(i) There is no term F_{C0} for the inelastic case.

(ii) The transverse electric terms of Eq. (5) are usually small. They have been assumed negligible and only the transverse magnetic terms have been used.

(iii) The coefficients α, β, and γ are parameters that are used to fit the data.

(iv) It is not possible to investigate the unresolved levels separately. However, two factors work in our favor in these cases. The transitions are predominated by Coulomb excitation with little or no transverse part. In addition, for our particular levels, the unresolved levels have different multipole transitions. For these reasons, the measured form factor is composed mostly of only two contributions, each with different functional behavior, so that the nuclear transition matrix element of the separate levels can be untangled from the whole. From the fit to each level, as shown in many papers,[3,7] it is possible to find the nuclear transition probabilities for radiative deexcitation, $B(\lambda, J_i, J_f)$ by evaluating the form factors in the limit $q \to 0$. Transition probabilities found in this way correspond to excitation of the level, and such a $B(\lambda, J_i, J_f)$ is identified as $B\uparrow$. The relation to the $B(\lambda, J_i, J_f)$ for deexcitation, $B\downarrow$, is through a statistical factor dependent on the spins, and is

$$B\downarrow = \frac{2J_i + 1}{2J_f + 1} B\uparrow . \tag{14}$$

J_i is the ground-state spin, and J_f is the excited-state spin.

The form factors for the various multipoles are

found by fitting the shell-model expressions (6) through (10) to the data. Once the contribution of a given multipole has been determined, these are related to the nuclear transition matrix elements. A typical equation is that for the $F_{C\lambda}{}^2(q^2)$'s, and is

$$F_{C\lambda}{}^2(q^2)=\frac{4\pi q^{2\lambda}}{[(2\lambda+1)!!]^2}\frac{B(C_\lambda, q, J_i, J_f)\uparrow}{Z^2e^2}. \quad (15)$$

The relations for the $F_{E\lambda}{}^2(q^2)$ and $F_{M\lambda}{}^2(q^2)$ are found in Ref. 3. We are actually seeking the nuclear transition probabilities which occur in the limit $q^2 \to 0$.

For the case $\lambda = 3$, as an example, $F_{C3}(q^2)/q^6$ is found from the fit of the data to Eq. (9), through evaluation of the parameter β. Finally, we have,

$$B(C_3, J_i, J_f)\uparrow \underset{q^2\to 0}{=} \frac{(7!!)^2}{4^4\pi} Z^2e^2\beta a^6 e^{-2d}. \quad (16)$$

This procedure is entirely model dependent, so that the result is not unique. However, if an appropriate model is chosen, a part of the arbitrariness is removed.

III. DATA ANALYSIS

A. Coulomb and Transverse Excitation

It has been pointed out by many authors,[2,7,8] that it is possible to distinguish the Coulomb excitation from a transverse excitation by measuring the cross sections at different electron energies for the same momentum transfer q. If $F^2(q^2, \theta)$ is independent of the angle θ, one has only a Coulomb excitation as seen in Eq. (3). If, on the other hand, $F^2(q^2, \theta)/(\frac{1}{2}+\tan^2\frac{1}{2}\theta)$ is independent of θ, one has predominantly a transverse excitation.

For the elastic N^{14} scattering there are points only up to the diffraction minimum at 250 MeV. It is seen in Fig. 4 that up to $q = 1.7$ F^{-1}, the points at 250 and 400 MeV fit reasonably well on one curve. Therefore, $F_L{}^2(q^2)$ is predominant in this range. In the same way, for N^{15} (Fig. 5), the points fit on one curve up to $q \simeq 1.6$ F^{-1}. Above $q = 1.6$ F^{-1}, the points no longer fit on one curve. It has been estimated that the transverse contribution represents 45% of the excitation at $q = 2$ F^{-1} compared with 55% longitudinal excitation. For the excited levels, shown in Figs. 6, 7, and 8, the excitation appears to be mainly longitudinal.

B. Determination of Parameters

The preceding paragraph shows that for the elastic scattering the first Coulomb term $F_{C0}(q^2)$ [Eq. (6)] predominates at low momentum transfer. The fit to these data was done in two steps. The first one was to determine the best value for the parameter a with a least-squares-fit program, using only the points with a q value less than that at the diffraction minimum. This is identical to the shell-model calculation of Ref. 1, with the difference that the coefficient α is fixed [$\alpha = \frac{1}{3}(Z-2) = 1.666$ for nitrogen]. This gives a value for the mean radius. For the complete study, additional multipoles are then introduced and all experimental points are taken into account. The main parameter a was initially set at the value found in the first step, and an iteration procedure was followed which determined the set of parameters with the best χ^2 value. The final value of a from the elastic scattering results was used in the calculations on the inelastic scattering.

As a criteria for the acceptability of the results, we required the χ^2 to have a reasonable value, and that relative contributions of the Coulomb transverse excitations that come from the fit be compatible with the results discussed in Sec. III A.

IV. RESULTS

A. Elastic Scattering on N^{14} and N^{15} with the Monopole Approximation

In order to establish an initial value for the parameter a, a best fit of the data was made to the

TABLE V. The parameters obtained from the best fit to the elastic scattering data using contributions from additional terms in the multipole expression of the form factors. See text for definitions. Errors are standard deviations weighted by χ^2.

Nucleus	Energy	a (F)	$\lvert\mu\rvert$ (μ_N)	α	$Q\times10^{24}$ (cm^2)	$\langle r\rangle$ (F)	χ^2	Degrees of freedom	μ static value (μ_N)	$Q\times10^{24}$ static value (cm^2)
N^{14}	400	1.75 ±1.2	30 ±65	0.44 ±0.35	(1.52±4.2) $\times10^{-2}$	2.64	38	10	0.4	2×10^{-2} [a] 7.1×10^{-2} [b]
N^{15}	250	1.74 ±0.2	2.5 ± 2.3	−0.64 ±0.4	0 (assumed)	2.65	42	14	0.28	0
	400	1.72 ±0.14	4.5 ± 3	−0.24 ±0.13	0 (assumed)	2.63	34	13	0.28	0

[a] E. Segrè, *Experimental Nuclear Physics* (John Wiley & Sons, New York, 1953), Vol. I, p. 435.
[b] *Handbook of Chemistry and Physics* (The Chemical Rubber Company, Cleveland, Ohio, 1967), 48th ed., p. E-69.

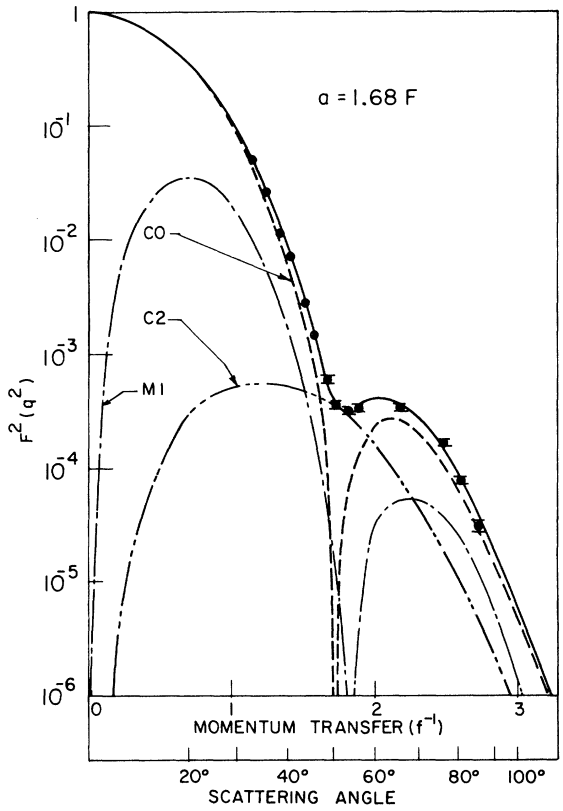

FIG. 9. The fit to the elastic scattering from N^{14} at 400 MeV using the shell-model description. The monopole ($C0$), magnetic dipole ($M1$), and electric quadrupole ($C2$) term contributions are shown in dashed lines. The solid curve is the total result of three terms.

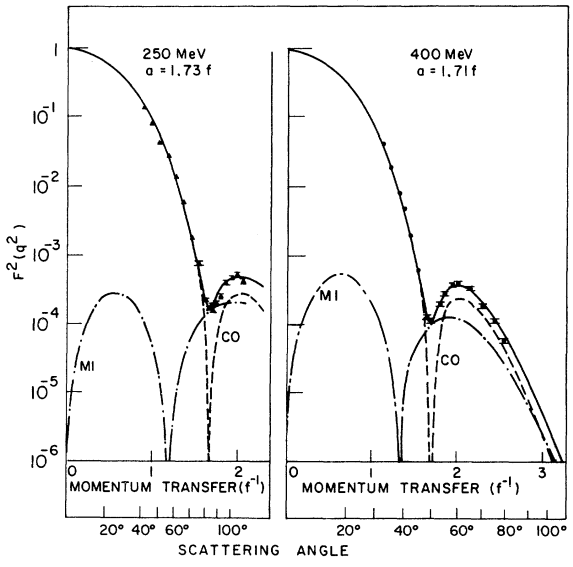

FIG. 10. The same as Fig. 9 for N^{15}. Only monopole ($C0$) and magnetic dipole ($M1$) terms contribute.

TABLE VI. The results of a phase-shift analysis for elastic electron scattering on N^{15} as found in Ref. 1. The parameters are shown for the shell model and Fermi models with two and three parameters. α is as defined in Ref. 1.

	Energy	a	α	$\langle r \rangle$
Shell model	250	1.71	2.26	2.61
(F_{C0} only)	400	1.75	1.72	2.59

	Energy	c	z	w	$\langle r \rangle$
Fermi	250	2.48	0.50	•••	2.67
Two parameter	400	2.43	0.50	•••	2.65
Fermi	250	2.23	0.48	0.32	2.71
Three parameter	400	2.32	0.50	0.14	2.70

first term, F_{C0} [Eq. (6)], in the form-factor expansion. Only points occurring before the diffraction minimum were used to find a value for a. The results of such a monopole fit to the N^{14} and N^{15} data are shown in Figs. 4 and 5, respectively.

B. Elastic Scattering on N^{14} and N^{15} with All Terms

The formulas (4)–(6), (11), and (12) were used and fitted with the parameters a, Q, μ, and α. The quadrupole moment of N^{15} is zero because the angular momentum is $J=\frac{1}{2}$. Nevertheless a fit has been tried, and a value $Q=0$ was found for the best fit. A final calculation assumed $Q=0$.

The results are given in Table V and in Figs. 9 and 10. For convenience we also show in Table VI a summary of the results for the elastic scattering of N^{15} obtained in Ref. 1. There we used the phase-shift analysis that evaluated the Fermi two- and three-parameter models and another version of the shell model.

In principle, μ and Q should represent the static magnetic dipole and electric quadrupole moments of the nucleus. The values found for μ and Q are not the same as the static moments of the nucleus.

C. Inelastic Scattering on N^{15}

The levels are excited primarily by the longitudinal mode, although it is possible to distinguish a transverse mode at high momentum transfer. The average value of a found from the elastic scattering at 250 and 400 MeV was used for the inelastic study. The results of the analysis are summarized in Table VII. The values of $B(\lambda, J_i, J_f)\downarrow$ found in this experiment are presented, as well as those of other sources.

(1) Doublet at $\epsilon_1=5.276$ and $\epsilon_2=5.304$ MeV. These levels are known to have angular momenta

$$J^\pi = \tfrac{5}{2}^+ \quad \text{for level at } \epsilon_1 = 5.276 \text{ MeV},$$

TABLE VII. Summary of the experimental results on the inelastic scattering from N^{15}. Column 1 is the level energy. The 250- and 400-MeV data were separately fitted to the 6.3-MeV transition when $M1$ was included in the fit. The 250- and 400-MeV data were combined for the fits to the other levels and for the fit to the 6.3-MeV level when $C2$ was used alone. Column 2 gives the possible transitions. These transitions in parentheses were not considered for the fits. Column 3 identifies the fitting parameters defined in the text, and column 4 gives their values. Column 5 is the χ^2/degree of freedom for the fits. Column 6 contains the values of $B(M\lambda, J_i, J_f)\downarrow$ found in this experiment. Column 7 has values of $B\downarrow$ found from other experiments, and lifetimes found in this experiment in column 8 can be compared with other experimental values in column 9 and the values obtained using an independent particle model (column 10). The errors are standard deviations weighted by the χ^2 of the fit.

Level	Mode of excitation	Fitted parameters: Parameter	Value	χ^2/degree of freedom	$B(M\lambda)\downarrow$ This expt.	Other expts.	Lifetimes τ (sec) This expt.	Other values	Weisskopf
5.27	$C3$ ($M2+E3$)	β	$(0.104\pm0.005)\times10^{-1}$	42.8/31	$(62.5\pm2.1)e^2$	$60e^2$ [a]	$(2.46\pm0.1)\times10^{-10}$	2.7×10^{-12} [b] $>10^{-12}$ [c] $>5\times10^{-12}$ [d]	11×10^{-10}
5.30	$C1$ ($E1$)	α	$(0.124\pm0.02)\times10^{-1}$		$(0.362\pm0.07)e^2$		$(1.16\pm0.2)\times10^{-17}$	4.3×10^{-14} [c] $<3\times10^{-13}$ [d]	1.1×10^{-17}
6.3	$C2$ ($M1+E2$)	α	$(0.369\pm0.02)\times10^{-1}$	66/33	$(4.03\pm0.14)e^2$	$4.9e^2$ [a]	$(1.97\pm0.2)\times10^{-14}$		2.23×10^{-14}
		α	$(0.325\pm0.04)\times10^{-1}$		$(3.49\pm0.3)e^2$	$4.9e^2$ [a]	$(2.18\pm0.3)\times10^{-14}$	1.1×10^{-14} [e] 1.65×10^{-14} [f] $<4.5\times10^{-14}$ [g]	2.23×10^{-14}
6.3 (250)	$C2+M1$ ($E2$)	β	(0.114 ± 0.06)	11.7/14	$(0.0853\pm0.04)e^2$		$(2.89\pm1.4)\times10^{-17}$	1.94×10^{-16} [e] 2.43×10^{-16} [f]	1.3×10^{-16}
		γ	(0.072 ± 0.04)						
6.3 (400)	$C2+M1$ ($E2$)	α	$(0.207\pm0.02)\times10^{-1}$		$(2.26\pm0.2)e^2$	$4.9e^2$ [a]	$(3.53\pm0.3)\times10^{-14}$		2.23×10^{-14}
		β	(0.168 ± 0.06)	6.1/13	$(0.182\pm0.06)e^2$		$(1.35\pm0.6)\times10^{-17}$		1.3×10^{-16}
		γ	(0.124 ± 0.06)						
7.30	$C1$ ($E1+M2$)	α	$(0.846\pm0.2)\times10^{-2}$		$(0.123\pm0.03)e^2$		$(1.30\pm0.3)\times10^{-17}$	$<2.5\times10^{-14}$ [g]	0.41×10^{-17}
7.56	$C3$ ($E3$)	β	$(0.124\pm0.004)\times10^{-1}$	33/31	$(56.0\pm1.6)e^2$	$60e^2$ [a]	$(2.19\pm0.07)\times10^{-11}$		9.2×10^{-11}

[a] B. G. Harvey, J. R. Meriwether, J. Mahoney, A. Bussiere de Nercy, and D. J. Horen, Phys. Rev. 146, 712 (1966).
[b] P. G. Bizzeti, A. M. Bizzeti-Sona, S. Kalbitzer, and B. Povh, Nucl. Phys. A104, 577 (1967).
[c] T. K. Alexander, A. E. Litherland, and C. Broude, Can. J. Phys. 43, 2310 (1965).
[d] E. K. Warburton, K. W. Jones, D. E. Alburger, C. Chasman, and R. A. Ristinen, Phys. Rev. Letters 14, 146 (1965).
[e] G. A. Beer, P. Brix, H.-G. Clerc, and B. Laube, Phys. Letters 26B, 506 (1968).
[f] A. R. Poletti, E. K. Warburton, and D. Kurath, Phys. Rev. 155, 1096 (1967).
[g] R. D. Gill, J. S. Lopes, O. Haussen, and H. J. Rose, Lifetime Measurements in Mass 15, Internal Report, Nuclear Physics Laboratory, University of Oxford, Oxford, England, 1968 (unpublished), Ref. 27/68.

and

$$J^\pi = \tfrac{1}{2}^+ \quad \text{for level at } \epsilon_2 = 5.304 \text{ MeV}.$$

For ϵ_1, the excitation can be obtained by transitions $C3$ and $M2+E3$. For ϵ_2, the excitation can be obtained by a transition $C1$. The data must be analyzed with the contribution of both levels together, because the experimental resolution is not enough to separate them. We neglect a contribution in $M2+E3$, which is assumed to be small compared with $C3$. Using formulas (3), (4), (7), and (9) (parameters α and β), the fit is shown in Fig. 6. The parameter α cannot be determined with much precision, because the $C3$-transition contribution dominates the form factor in the range of q covered by this experiment. Therefore one has a larger uncertainty on the nuclear transition probability of the level at 5.30 MeV.

(2) Level at $\epsilon = 6.328$ MeV. The angular momentum is $J = \frac{3}{2}^-$. A first analysis has been done by neglecting the transverse contribution and assuming that the parity is not known, the curves have been plotted for excitation by $C1$ (if $J = \frac{1}{2}$ or $\frac{3}{2}$), $C2$ (for $J = \frac{3}{2}$ or $\frac{5}{2}$), and $C3$ (for $J = \frac{5}{2}$) using Eqs. (7), (8), and (9). The result is shown in Fig. 7. It is clear that the curves using only $C2$ as a first approximation are closest to the data. However, the $C2$ curve deviates badly from the data points at higher q. In order to try to improve the fit, the analysis was repeated with the addition of a magnetic dipole term $M1$ [from Eqs. (4), (5), (8), and (10)]. This is done separately for the 250- and 400-MeV data because of the angular dependence. The result is shown in Fig. 11, and the over-all fit is considerably improved. The need for an $M1$ term seems clear, and the angular momentum is $J^\pi = \frac{3}{2}^-$.

(3) Levels at $\epsilon_1 = 7.16$, $\epsilon_2 = 7.30$, and $\epsilon_3 = 7.57$ MeV. The position of the envelope of the three peaks (see Figs. 1 and 2) implies that the level at 7.16 MeV is not strongly excited. Therefore we have fitted the experimental points with the levels at 7.30 MeV ($J^\pi = \frac{3}{2}^+$) and 7.57 MeV ($J^\pi = \frac{7}{2}^+$). We have again neglected the transverse contribution and have used longitudinal contributions $C1$ (for 7.30 MeV) and $C3$ (for 7.57 MeV). The formulation is then identical to that of the doublet 5.27-5.30 MeV. The fit is shown in Fig. 8. Here, as in the 5.3-MeV doublet, the $C3$ transition is better determined, because of its dominance, so that $B\downarrow$ of the 7.3-MeV level is less well known.

V. CONCLUSION

Our fits to the elastic scattering data (Table V) using the shell model yield large values of χ^2. In each case, about one third of the χ^2 value arises from one data point. However the χ^2 would still remain rather large. This is consistent with our findings in Ref. 1. There, the phase-shift calculations for the Fermi models (away from the minimum) gave better fits than the shell model. Thus, although through the use of the various multipole moments of the shell model we have been able to fill in the minima in the data, the model does not yield satisfactory fits. In addition the magnetic moments required to make the fits are an order of magnitude or more larger than the known static moments. Such behavior was anticipated as a result of our previous work. The reason for this is not understood.

The errors attached to the values of the parameters in Table V are the standard deviations found from the error matrix, weighted by the χ^2 of the fit. These parameters are highly correlated, especially μ and α. The errors given for the N^{14} parameters are especially large because we have attempted to fit four parameters with a limited amount of data.

The value of a for N^{14} is considerably larger than that found by Bishop, Bernheim, and Kossanyi-Demay,[9] whose measurements did not extend to the diffraction minimum. If we confine our fit to the term $F_{C0}(q^2)$ [Eq. (6)] and use data in the q^2 region below the diffraction minimum, then we find $a = 1.68$ F, to be compared with $a = 1.67$ F from Ref. 9. This fit is shown in Fig. 4. Inclusion of the additional terms forces the value of a higher. The $M1$ term compensates for the decrease in the cross section that occurs at low q^2.

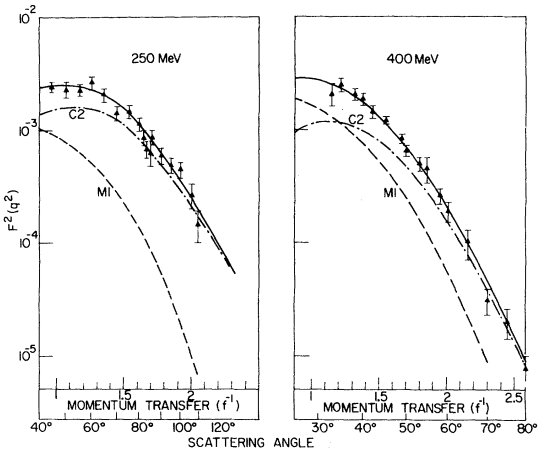

FIG. 11. The 6.3-MeV-level data at 250 and 400 MeV fitted with an $M1$ contribution in addition to the $C2$ multipole.

The fits to the elastic scattering from N^{15} give an a value that is very consistent between the 250- and 400-MeV data and compares favorably with the value found in Ref. 1 for the $F_{C0}(q^2)$ term. Whether or not the near equality of the a and $\langle r \rangle$ values for N^{14} and N^{15} is real or not cannot be answered by our data.

The results from the inelastic scattering are summarized in Table VII. The agreement with values of $B\downarrow$ and the lifetimes from other experiments is good for the doublet at 5.3 MeV and the triplet of levels at 7.3 MeV. The values of $B\downarrow$ and τ for the $C2$ part of the 6.3-MeV transition are in good agreement with previous results. However, our result for the $M1$ part is an order of magnitude different from other experiments. The errors shown in Table VII were determined the same way as the errors for the elastic scattering parameters.

ACKNOWLEDGMENTS

We want to acknowledge the assistance that we received from many people in performing this experiment. In particular, one of us (M.C.) wishes to thank Professor Hofstadter of Stanford University for the support during his stay, and for the use of the facilities of the Hansen Laboratory. The initial (and an essential) part of this work was done at the Institute de Recherches Nucléaires, Strasbourg, France. One of us (E.D.) is thankful to Professor Gorodetzky of that institute for the unlimited use of the laboratory during his residence there.

*Work supported in part by the U. S. Office of Naval Research, Contract No. [Nonr 225(67)].

†Present address: Stanford Linear Accelerator Center, Stanford, California 94305.

[1]E. B. Dally, M. G. Croissiaux, and B. Schweitz, Phys. Rev. 188, 1590 (1969).

[2]T. De Forest and J. D. Walecka, Advan. Phys. 15, 1 (1966).

[3]R. S. Willey, Nucl. Phys. 40, 529 (1963).

[4]G. R. Bishop, in *Nuclear Structure and Electromagnetic Interactions*, edited by N. MacDonald (Oliver and Boyd, Edinburgh and London, England, 1964), p. 24.

[5]T. Stovall, D. Vinciguerra, and M. Bernheim, Nucl. Phys. A91, 513 (1967).

[6]L. J. Tassie and F. C. Barker, Phys. Rev. 111, 940 (1958).

[7]L. J. Tassie, Nuovo Cimento 5, 1497 (1957).

[8]K. Alder, A. Bohr, T. Huus, B. Mottelson, and A. Winther, Rev. Mod. Phys. 28, 432 (1956), p. 475.

[9]G. R. Bishop, M. Bernheim, and P. Kossanyi-Demay, Nucl. Phys. 54, 353 (1964).

PHYSICAL REVIEW C VOLUME 2, NUMBER 6 DECEMBER 1970

Evidence of $E2$ and $M1$ Transitions in High-Energy Photonuclear Reactions in O^{16}

M. G. Mustafa*
Electron Accelerator Laboratory, Physics Department, Yale University, New Haven, Connecticut 06520

and

F. B. Malik†
Physics Department, Indiana University, Bloomington, Indiana 47401

(Received 6 July 1970)

The observed forward-peaked angular distributions and polarization at 90° of photonucleons from O^{16} are ascribed to the interference of $E1$ and $(E2+M1)$ transitions within the context of a direct-reaction model, using wave functions computed in a Woods-Saxon potential.

I. INTRODUCTION

Data[1,2] on high-energy photonucleon yields from O^{16} at energies above "the giant dipole" region admit a fairly simple analysis on the basis of a direct-reaction model, assuming a pure $E1$ nature for this transition.[3,4] In the context of this model, the differential photonucleon cross section at a given energy should be peaked at 90° and symmetric about this point. In addition, for a pure $E1$ transition, the nucleon polarization at 90° should be zero. Recent data on angular distributions[5,6] and the polarization at 90°[7-9] contradict the last two general predictions of the direct-reaction model, which, on the other hand, reproduces the correct magnitudes of both the differential and the integrated cross section. The purpose of this paper is to point out that, within the framework of this direct-reaction model, both of these phenomena indicate the presence of other multipole transitions in the photonucleon yields. In particular, the interference of the $E2$ and $E1$ transitions is the primary cause of the observed angular distribution[10] and polarization data.

II. MODEL

The pertinent formulas for the photonuclear cross sections of any multipole electromagnetic transition of the order L caused by the absorption of an incident photon of energy E_γ and momentum $\vec{k}_\gamma$ (defined with respect to the momentum vector $\vec{k}$ of the outgoing nucleon) by a target nucleus of spin I is easily obtained by generalizing expressions for $E1$ transitions given in earlier works.[4,11,12] Thus the differential cross section is given by

$$\frac{d\sigma}{d\Omega}(\vec{k}_\gamma,\vec{k})=\frac{1}{\hbar v(2I+1)}\sum_{\substack{LL'\lambda\lambda'Q\\ l_f l_f' j_f j_f'}}\left[\frac{(L+1)(L'+1)}{LL'}\right]^{1/2}\frac{1}{(2L-1)!!(2L'-1)!!}\left(\frac{E_\gamma}{\hbar c}\right)^{L+L'-1}(-1)^{\frac{1}{2}(l_f-l_f'-Q)+P+P'+j_i+\frac{1}{2}}$$

$$\times\tfrac{1}{2}[1+(-1)^{l_f+l_f'+Q}](LL'-11|Q0)W(j_fLj_f'L';j_iQ)Z(l_fj_fl_f'j_f';\tfrac{1}{2}Q)A_L(\lambda)A_{L'}{}^*(\lambda')P_Q(\cos\theta)\,, \qquad (1)$$

and similarly the integrated cross section is